

Design and Analysis of Discrete-Time Repetitive Control for Scanning Probe Microscopes

Ugur Aridogan

Yingfeng Shan

Kam K. Leang¹

e-mail: kam@unr.edu

Department of Mechanical Engineering,
University of Nevada-Reno,
Reno, NV 89557

This paper studies repetitive control (RC) with linear phase lead compensation to precisely track periodic trajectories in piezo-based scanning probe microscopes (SPMs). Quite often, the lateral scanning motion in SPMs during imaging or nanofabrication is periodic. Dynamic and hysteresis effects in the piezoactuator cause significant tracking error. To minimize the tracking error, commercial SPMs commonly use proportional-integral-derivative (PID) feedback controllers; however, the residual error of PID control can be excessively large, especially at high scan rates. In addition, the error repeats from one operating cycle to the next. To account for the periodic tracking error, a discrete-time RC is designed, analyzed, and implemented on an atomic force microscope (AFM). The advantages of RC include straightforward digital implementation and it can be plugged into an existing feedback control loop, such as PID, to enhance performance. The proposed RC incorporates two phase lead compensators to ensure robustness and minimize the steady-state tracking error. Simulation and experimental results from an AFM system compare the performance among (1) PID, (2) standard RC, and (3) the modified RC with phase lead compensation. The results show that the latter reduces the steady-state tracking error to less than 2% at 25 Hz scan rate, an over 80% improvement compared with PID control. [DOI: 10.1115/1.4000068]

1 Introduction

This paper specifically addresses the repetitive tracking error in scanning probe microscopes (SPMs) through the design and application of a plug-in repetitive control (RC) system. Scanning probe microscopes, for example an atomic force microscope (AFM), typically employ piezoactuators to position the tool tip (probe) relative to a specimen for surface interrogation and modification [1]. Quite often, the positioning of the SPM probe follows a periodic trajectory. For example, during AFM imaging a triangle input signal is applied to the piezoactuator to raster the cantilever probe back and forth over the sample surface. As the probe moves over the surface, the tip-to-sample interaction, for instance the vertical deflection of the cantilever, is measured and used to construct an image of the sample's topology [2]. Likewise, in nanindentation a SPM probe is scanned repeatedly across the sample surface and at specific time instances the probe is lowered to create nano-sized indents [3]. During the scanning operation, hysteresis and dynamic effects in the piezoactuator cause significant positioning error that repeats from one operating cycle to the next [4,5]. Unfortunately, the error causes distortion in images and fabricated features [1], and therefore limits the performance of SPMs. It is pointed out that in nanofabrication, the size, shape, and spacing of nano features are important to their functionality. As a result, precise control of the positioning of the SPM-probe tip is needed for fabricating uniformly distributed patterns of nano-sized features for the growth and investigation of novel structures; and to obtain high-resolution, undistorted images of the sample [6]. A discrete-time repetitive controller is proposed to account for the periodic tracking error. The main contributions of this paper include the analysis of the performance of discrete-time RC for SPM from a practical viewpoint and experimentally investigating the performance of RC on an AFM system. As previously men-

tioned, an advantage of the proposed plug-in RC system is that it can be easily integrated into an existing feedback controller in SPMs to handle tracking error due to periodic motion and/or to reject periodic exogenous disturbances. The proposed repetitive controller consists of two simple phase lead compensators, one to ensure robustness and the other to minimize the steady-state tracking error.

Repetitive control, a concept based on the internal model principle [7], is suited for tracking periodic trajectories [8,9]. Compared to traditional proportional-integral (PI) or proportional-integral-derivative (PID) feedback controllers for SPM [10], where careful tuning is required and the residual tracking error due to hysteresis and dynamic effects persists from one operating cycle to the next, RC has the ability to reduce the error as the number of operating cycles increases [11]. The RC approach achieves precise tracking of a periodic reference trajectory by incorporating a signal generator within the feedback loop—the signal generator provides infinite gain at the fundamental frequency of the reference trajectory and its harmonics. Such a controller has been investigated to address run-out issues in disk drive systems [11,12], to generate AC waveforms with low harmonic distortion [13], and to improve the performance of machine tools [14,15]. However, past work on RC for piezo-based systems and SPMs is limited [16], but it includes a feedback-linearized controller with RC for a piezopositioning stage [17]. This work specifically considers the RC approach for AFM and its implementation in discrete time.

A repetitive controller offers many advantages for SPM applications. For one, it can be plugged into an SPM's existing feedback controller to enhance performance for scanning operations. When the piezoactuator scans at a location offset from its center position, the periodic tracking error during scanning can be handled by the repetitive controller, and the resident PID controller, can be used to account for low frequency dynamics such as creep or drift [18]. But when the reference trajectory is not periodic, the RC controller can be disabled to allow the feedback controller (and/or a feedforward-based controller [6]) to compensate for the tracking error. Compared to iterative learning control (ILC) [19,20], which is an effective approach that exploits the

¹Corresponding author.

Contributed by the Dynamic Systems, Measurement, and Control Division of ASME for publication in the JOURNAL OF DYNAMIC SYSTEMS, MEASUREMENT, AND CONTROL. Manuscript received May 30, 2008; final manuscript received May 22, 2009; published online October 30, 2009. Editor: J. Karl Hedrick.

process of repetition to compensate for hysteresis and dynamic effects in piezoactuators [21,22], RC does not require the initial condition to be reset at the start of each iteration trial [9]. Resetting the initial conditions adds another level of complexity during implementation. Furthermore, the design and implementation of RC does not require extensive modeling of the system, where as model-based approaches require relatively accurate models of the dynamics and nonlinearities [6]. One of the disadvantages with open-loop feedforward control is the lack of robustness due to variations in the system dynamics, for instance under cyclic loading [23], with aging effects [24], or through temperature variations [25]. On the other hand, the feedback mechanism built into RC provides robustness to parameter variation. At the expense of reduced modeling, the RC approach does require accurate knowledge of the period of the reference trajectory. But in SPMs used for scanning-type applications such as imaging and nanofabrication, the reference signal's period is often known in advance. Another advantage of RC is that it can be easily implemented on a microprocessor as it does not require the inversion of a system model. Therefore, newly available high-speed data acquisition and control hardware [26] can take advantage of the simplicity of RC. This means that RC is attractive for controlling video-rate AFM imaging systems with the available high-speed digital hardware [27,28]. Analog circuit designs have been proposed for implementing RC [29].

In the design and application of RC, the major challenges are stability, robustness, and good steady-state tracking performance. The stability and robustness problems have been addressed by incorporating a low-pass filter in the RC loop [30]. Likewise, a simple frequency aliasing filter can be used to stabilize RC and this approach has been applied to a gantry robot [31]. However, a tradeoff is made between robustness and high-frequency tracking when such filters are used. The steady-state tracking performance of RC was considered in Refs. [32,33] by cascading a compensator to account for the phase of the low-pass filter. Also, high-order RC was studied in Ref. [12] to improve performance and robustness in the presence of noise and variations in period-time. The design of pole-placement RC was considered in Ref. [34]. In light of previous work on RC, this paper focuses on designing an RC system that is both robust and achieves minimum steady-state error. Easy-to-tune linear phase lead compensators are incorporated into the RC design to enhance performance. One advantage of the phase lead compensators is they can be easily implemented in discrete time; therefore, the design can be plugged into existing SPMs to control the positioning of the piezoactuator. The effects

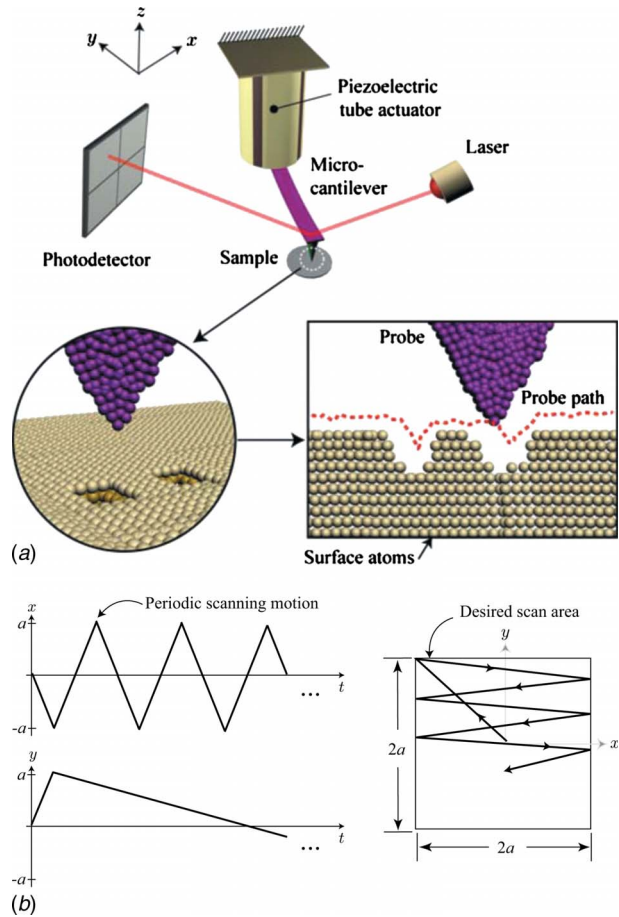


Fig. 1 The atomic force microscope (AFM): (a) A schematic of the main components and (b) typical scan paths in the lateral directions during AFM imaging

of the RC parameters are analyzed and suggestions for how to tune them are provided. Lastly, the performance of RC is demonstrated on a piezoactuator used in a commercial AFM system.

The remainder of this paper is organized as follows. First, in Sec. 2, the basic operation of AFM is presented to show the con-

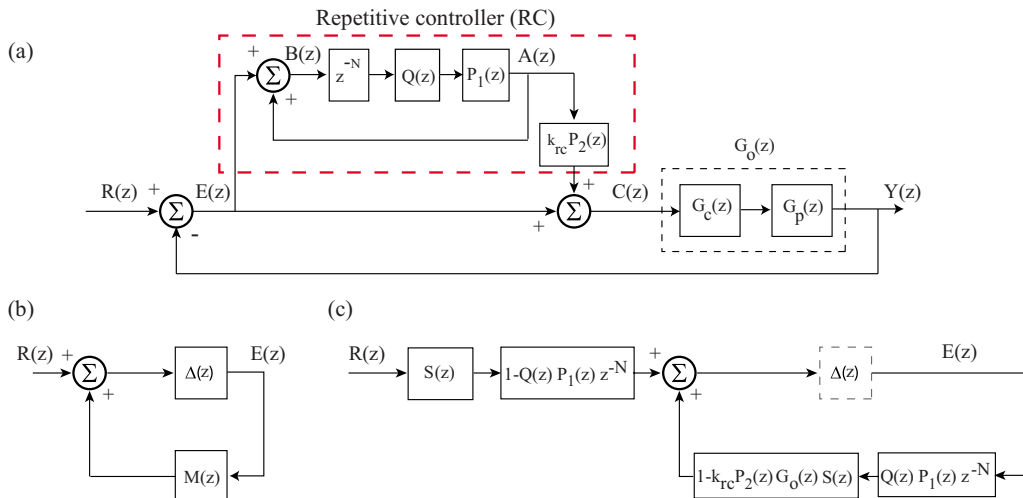


Fig. 2 The repetitive control (RC) feedback system: (a) The block diagram of the proposed RC system, (b) positive feedback system for stability analysis, and (c) positive feedback system representing the block diagram in part (a) for stability analysis

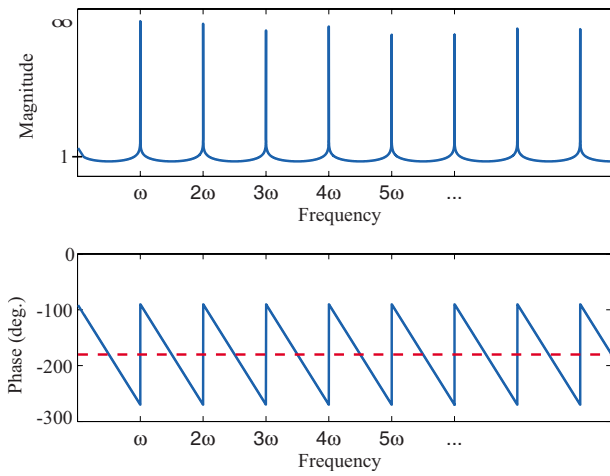


Fig. 3 Magnitude and phase versus frequency for signal generator $z^N/(1-z^N)$, where $z=e^{j\omega T_s}$

control problem of interest. Then, Sec. 3 discusses the RC method and the analysis of the proposed RC design for AFM. Sections 4 and 5 discuss the simulation and experimental results on AFM tracking and imaging. Finally, Sec. 6 offers the concluding remarks.

2 Atomic Force Microscopy

In AFM, a microcantilever (with a sharp tip at its distal end) is positioned relative to a sample using a piezoactuator as shown in Fig. 1(a). The piezoactuator positions the AFM probe tip along the x , y , and z axes. For example, in the contact, constant-height imaging mode, the piezoactuator rasters the tip laterally (x and y) at a fixed height above the sample surface. The x and y scanning motions are shown in Fig. 1(b). As the tip moves over the sample surface, the tip-to-sample interaction causes, for instance, the cantilever to deflect. The cantilever's deflection is measured with a laser and photodetector. The cantilever's deflection is used to construct an image of the sample's surface. The AFM is also used for surface modification and metrology [1].

One of the major performance limitations of AFM is tracking errors between the AFM probe and sample surface in the lateral and vertical directions. The errors lead to excessive tip-to-sample forces, causing image distortion, and in nanofabrication, causing poor dimensional tolerance of fabricated features. For scanning applications such as imaging, precision tracking of the periodic

scanning motion is needed to obtain accurate images of the surface topology. Therefore, the control objective is to precisely track the periodic lateral scanning motion (see Fig. 1(b)).

3 Repetitive Control Design and Analysis

Repetitive control is a direct application of the internal model principle [7], where high-accuracy tracking of a desired periodic trajectory, with period T_p , is achieved if the controller consists of the transfer function of the reference trajectory [8,9,30]. One such controller is a signal generator with period T_p .

The discrete-time closed-loop system with RC for the AFM system in consideration is shown in Fig. 2(a). The piezoactuator dynamics, assumed to be linear, are represented by $G_p(z)$, where $z=e^{j\omega T_s}$, $\omega \in (0, \pi/T_s)$. In the block diagram, $G_c(z)$ is a feedback controller, such as a resident PID controller in the SPM; $Q(z)$ is a low-pass filter for robustness; k_{rc} is the RC gain; and $P_1(z)=z^{m_1}$ and $P_2(z)=z^{m_2}$, where m_1, m_2 are non-negative integers, are positive phase lead compensators to enhance the performance of the RC feedback system. It is emphasized that the phase lead compensators z^{m_1} and z^{m_2} provide a linear phase lead of (in units of radians)

$$\theta_{1,2}(\omega) = m_{1,2}T_s\omega \quad (1)$$

for $\omega \in (0, \pi/T_s)$.

To create a signal generator with period T_p , the repetitive controller in the inner loop contains the pure delay z^{-N} , where the positive integer $N=T_p/T_s$ is the number of points per period T_p ; and T_s is the sampling time. An analysis of the performance of the closed-loop system is presented below, where the following assumptions are considered.

ASSUMPTION 1. The reference trajectory $R(z)$ is periodic and has period T_p .

ASSUMPTION 2. The closed-loop system without the RC loop is asymptotically stable, i.e., $1+G_c(z)G_p(z)=0$ has no roots outside of the unit circle in the z -plane.

Remark 1. Assumptions 1 and 2 are easily met for SPMs. For example, during scanning applications such as imaging, the lateral movements of the piezoactuator are periodic, such as a triangle scanning signal (see Fig. 1(b)). Also, most SPMs are equipped with feedback controllers $G_c(z)$ to control the lateral positioning, which can be tuned to be stable.

The transfer function of the signal generator (or RC block, Fig. 2(a)) that relates $A(z)$ to $E(z)$ is given by

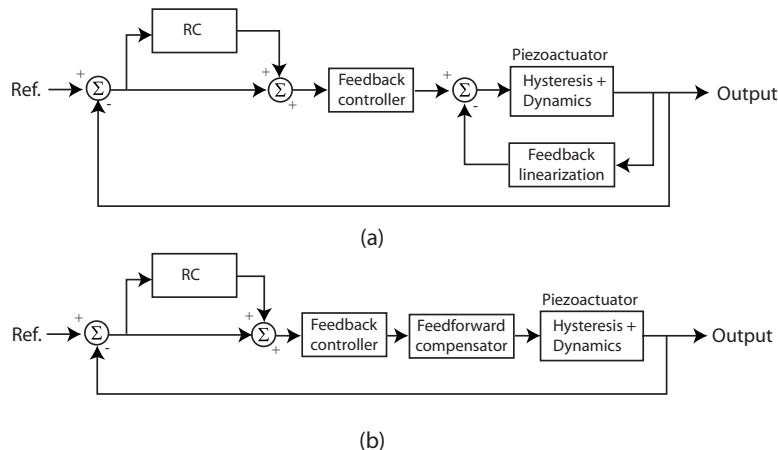


Fig. 4 Techniques to account for hysteresis in RC design: (a) Feedback-linearization approach and (b) feedforward hysteresis compensation [38]

$$\frac{A(z)}{E(z)} = \frac{Q(z)P_1(z)z^{-N}}{1 - Q(z)P_1(z)z^{-N}} = \frac{Q(z)z^{(-N+m_1)}}{1 - Q(z)z^{(-N+m_1)}} \quad (2)$$

In the absence of both the low-pass filter $Q(z)$ and positive phase lead $P_1(z)=z^{m_1}$, the poles of the signal generator are $1-z^{-N}=0$; therefore, the frequency response of the signal generator shown in Fig. 3 reveals infinite gain at the fundamental frequency and its harmonics $\omega=2n\pi/T_p$, where $n=1,2,3,\dots$. The infinite gain at the harmonics is what gives the RC its ability to track a periodic reference trajectory. As a result, RC is a useful control method for SPM in which the scanning motion is repetitive, such as the lateral probe motion during AFM imaging. Unfortunately, the RC also contributes phase lag which causes instability. Therefore, the stability, robustness, and tracking performance of the RC closed-loop system must be carefully considered. In the following, these issues will be addressed, and the conditions for how to choose the RC gain k_{rc} are presented, along with a discussion of the effects of the phase lead compensators $P_1(z)$ and $P_2(z)$ on the performance of the closed-loop system.

3.1 Stability of RC System. To analyze the stability of the closed-loop RC system shown in Fig. 2(a), consider the transfer function relating the tracking error $E(z)$ and the reference trajectory $R(z)$,

$$\frac{E(z)}{R(z)} = \frac{1 - H(z)}{1 - H(z) + [(k_{rc}P_2(z) - 1)H(z) + 1]G_o(z)} \quad (3)$$

where $H(z)=Q(z)z^{(-N+m_1)}$ and $G_o(z)=G_c(z)G_p(z)$. Multiplying the numerator and denominator of Eq. (3) by the sensitivity function $S(z)=1/(1+G_o(z))$ of the feedback system without the repetitive controller, the following transfer function is obtained

$$S_{rc}(z) = \frac{E(z)}{R(z)} = \frac{[1 - H(z)]S(z)}{1 - H(z)[1 - k_{rc}P_2(z)G_o(z)S(z)]} \quad (4)$$

The $S_{rc}(z)$ shown above is referred to as the sensitivity function of the closed-loop RC system.

The stability conditions for the RC system can be determined by simplifying the block diagram in Fig. 2(a) to the equivalent interconnected system shown in Fig. 2(b), which results in Fig. 2(c). Then the RC sensitivity transfer function (4) can be associated with the $M(z)$ and $\Delta(z)$ terms in Fig. 2(c) for stability analysis.

ASSUMPTION 3. $1-H(z)$ is bounded input-bounded output stable.

By Assumption 2, the sensitivity function without RC, $S(z)$, has no poles outside the unit circle in the z -plane, so it is stable. Likewise by Assumption 3, $1-H(z)$ is stable. Replacing $z=e^{j\omega T_s}$, the positive feedback closed-loop system in Fig. 2(c) is internally stable according to the small gain theorem [35] when

$$\begin{aligned} & |H(z)[1 - k_{rc}P_2(z)G_o(z)S(z)]| \\ &= |H(e^{j\omega T_s})[1 - k_{rc}e^{j\theta_2(\omega)}G_o(e^{j\omega T_s})S(e^{j\omega T_s})]| < 1 \end{aligned} \quad (5)$$

for all $\omega \in (0, \pi/T_s)$, where the phase lead $\theta_2(\omega)$ is defined by Eq. (1). By satisfying condition (5), the closed-loop RC system shown in Fig. 2(a) is asymptotically stable.

In general, both the RC gain k_{rc} and the phase lead $\theta_2(\omega)$ affect the stability and robustness of RC as well as the rate of convergence of the tracking error. In the following, condition (5) is used to determine explicitly the range of acceptable k_{rc} for a given $Q(z)$ and $G_o(z)$. The effects of the phase lead $\theta_2(\omega)$ on robustness and the phase lead $\theta_1(\omega)$ on the tracking performance will be discussed.

3.2 The RC Gain and Robustness. Let $T(z)$ represent the complimentary sensitivity function of the closed-loop feedback system without RC, that is, $T(z)=G_o(z)S(z)$. Suppose the magni-

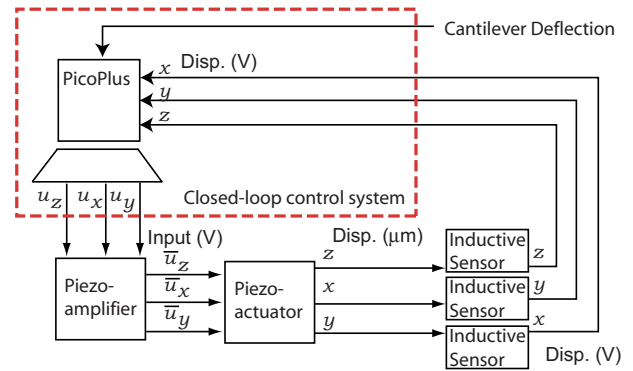


Fig. 5 A block diagram of the experimental AFM system. An external computer running custom c code was used to implement the control algorithm.

tude of the low-pass filter $|Q(z)|$ approaches unity at low frequencies and zero at high frequencies, hence $|Q(e^{j\omega T_s})| \leq 1$, for $\omega \in (0, \pi/T_s)$. Therefore, condition (5) becomes

$$|1 - k_{rc}e^{j\theta_2(\omega)}T(e^{j\omega T_s})| < 1 \leq \frac{1}{|Q(e^{j\omega T_s})|} \quad (6)$$

Replacing the complimentary sensitive function with $T(e^{j\omega T_s})=A(\omega)e^{j\theta_T(\omega)}$, where $A(\omega)>0$ and $\theta_T(\omega)$ are the magnitude and phase of $T(e^{j\omega T_s})$, respectively, Eq. (6) becomes

$$|1 - k_{rc}A(\omega)e^{j[\theta_T(\omega)+\theta_2(\omega)]}| < 1 \quad (7)$$

Noting that $e^{j\theta}=\cos(\theta)+j\sin(\theta)$ and $k_{rc}>0$, Eq. (7) simplifies to

$$-2k_{rc}A(\omega)\cos[\theta_T(\omega)+\theta_2(\omega)]+k_{rc}^2A^2(\omega) < 0 \quad (8)$$

which leads to the following two conditions for the RC gain k_{rc} and linear phase lead $\theta_2(\omega)$ to ensure stability:

$$0 < k_{rc} < \frac{2\cos[\theta_T(\omega)+\theta_2(\omega)]}{A(\omega)} \quad (9)$$

and

$$-\pi/2 < [\theta_T(\omega)+\theta_2(\omega)] < \pi/2 \quad (10)$$

By Eq. (10), the lead compensator $P_2(z)=z^{m_2}$ accounts for the phase lag of the closed-loop feedback system without RC. In fact, $P_2(z)$ enhances the stability margin of the closed-loop RC system by increasing the frequency at which the phase angle crosses the ± 90 deg boundaries. This frequency will be referred to as the crossover frequency.

The RC gain k_{rc} can be designed to take into account uncertainties in the plant model. In particular, consider an overall model uncertainty for the closed-loop system (without RC) of the following form:

$$T_a(z) = T(z)[1 + \Delta(z)] \quad (11)$$

where $\|\Delta(z)\| \leq \gamma$. Taking this into account, condition (9) becomes

$$0 < k_{rc} < \frac{2\cos[\theta_{T_a}(\omega)+\theta_2(\omega)]}{A(\omega)[1+\gamma]} \quad (12)$$

Hence, the value of the RC gain k_{rc} is inversely proportional the size of the plant uncertainty. In summary, the effects of unmodeled dynamics can be taken into account by choosing a relatively conservative RC gain through Eq. (12).

In the above analysis, the effects of hysteresis were not considered explicitly in the RC design. To keep the analysis simple, an approach to minimize the affect of hysteresis for RC is optimizing the resident feedback controller $G_c(z)$ in such a way that the closed-loop performance accounts for the hysteresis behavior over the bandwidth of interest. This is the approach considered in this

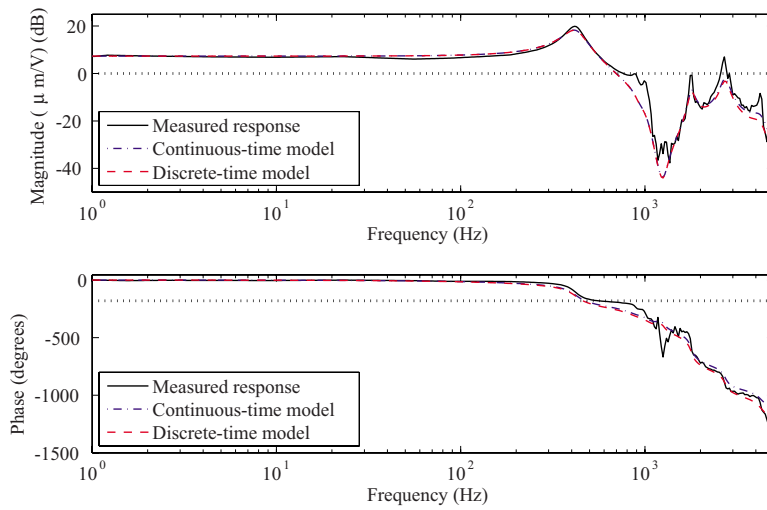


Fig. 6 The frequency response of piezoactuator along the x -axis. The solid line is the measured response, the dash-dot line represents the linear continuous-time model $G(s)$, and the dash line is the linear discrete-time model $G_p(z)$ using MATLAB function `c2d` with zero-order hold and sampling frequency of 10 kHz.

work. Additionally, it has been shown that high-gain feedback control is effective for significantly reducing hysteresis behavior [36], therefore, keeping γ as small as possible. Another approach is depicted in Fig. 4(a), where an internal feedback loop is used to linearize the plant dynamics [17]. Likewise, the hysteresis can be accounted for using model-based feedforward compensation as illustrated in Fig. 4(b) [37,38]. Therefore, compensating for the hysteresis effect permits the application of the analysis presented above.

3.3 Tracking Performance. Aside from designing RC for stability, it is important to also consider the degree by which the tracking error is reduced relative to the tracking error of the original feedback system (without RC). By Assumption 1 where the reference trajectory $R(z)$ is periodic, the tracking performance of RC can be analyzed by examining the sensitivity function of the RC system at the frequency multiples of the fundamental, $\omega = k(2\pi/T_p) = k\omega_p$ for $k=1,2,3,\dots$, within the bandpass of the low-pass filter $Q(z)$.

Recalling Eq. (4), the magnitude of the tracking error at multiples of the fundamental ω_p is given by

$$\begin{aligned}
 |E(e^{jk\omega_p})| &= |S_{rc}(e^{jk\omega_p})R(e^{jk\omega_p})| \\
 &\leq \left| \frac{1 - H(e^{jk\omega_p})}{1 - H(e^{jk\omega_p})[1 - k_{rc}P_2(e^{jk\omega_p})G_o(e^{jk\omega_p})S(e^{jk\omega_p})]} \right| |S(e^{jk\omega_p})| \\
 &\quad \times |R(e^{jk\omega_p})| \\
 &\leq |W(e^{jk\omega_p})| \times |S(e^{jk\omega_p})| \times |R(e^{jk\omega_p})| \quad (13)
 \end{aligned}$$

where $W(e^{jk\omega_p})$ is the effect due to the RC. Ideally without the low-pass filter $Q(z)$, $|W(e^{jk\omega_p})|=0$ at the multiples of the fundamental frequency ω_p . However, the addition of $Q(z)$ for stability causes phase lag in the RC, which shifts the point of maximum gain of the signal generator created by the pure delay z^{-N} [17,32]. Such a shift inadvertently lowers the RC gain at the harmonics and thus negatively affects the tracking performance of the RC system. But most of the phase lag can be accounted for using the linear phase lead $\theta_1(\omega)$ in the RC loop to improve the tracking performance [33]. Because $N \gg m_1$, the modified delay $z^{-(N+m_1)}$ is causal and can be easily implemented on a microprocessor. Therefore, the value of the phase lead $\theta_1(\omega)$ can be adjusted through m_1 to minimize the factor $|W(e^{jk\omega_p})|$ over the frequency range of the

bandpass of $Q(z)$. It is shown below that such a tuning process can be done in simulation and then implemented on the experimental system.

4 Design of RC for AFM Scanning

The repetitive control system in Fig. 2(a) was implemented on a commercial AFM system. The details of the implementation and experimental results are presented below. First, the AFM system and the modeling of the piezoactuator linear dynamics are described. Then a simulation study is presented before implementing the discrete-time RC for AFM scanning.

4.1 The AFM System. The AFM system is the Molecular Imaging (now part of Agilent Technologies, Santa Clara, California) PicoPlus model. The block diagram of the AFM and control system is shown in Fig. 5. The AFM uses a piezoelectric tube-shaped actuator for positioning the cantilever and probe tip (see Fig. 1(a)). The AFM was customized to permit the application of control signals to control the movement of the piezoactuator in the

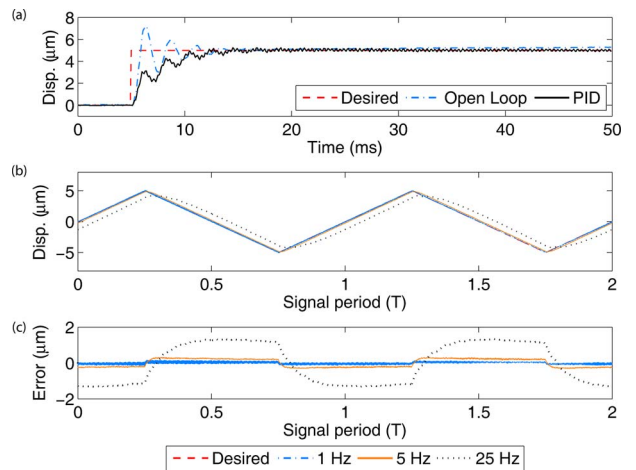


Fig. 7 The measured responses of the PID controller to (a) a step reference and (b) triangle references at 1 Hz, 5 Hz, and 25 Hz. (c) The tracking error for the triangle reference signals associated with plot (b).

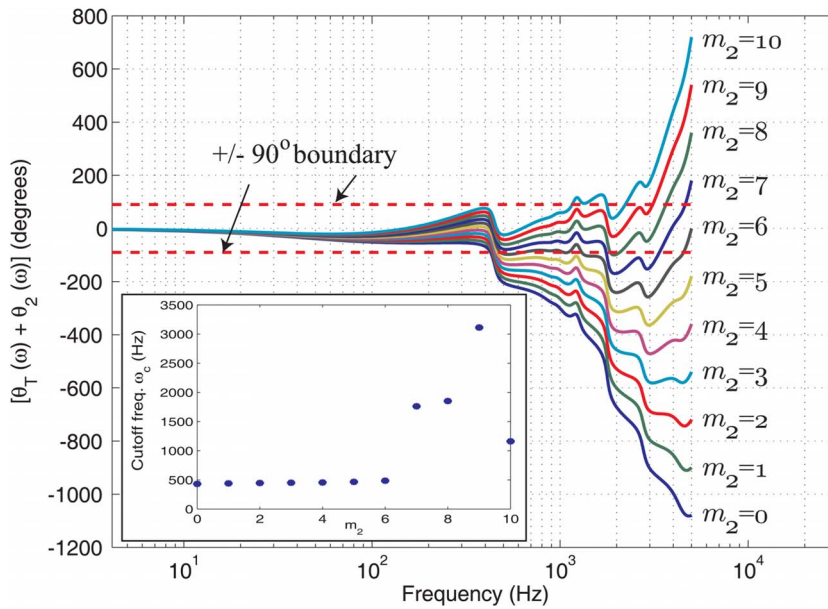


Fig. 8 The phase response of the closed-loop feedback system without RC and added phase lead $\theta_2(\omega)$, stability condition Eq. (10). The inset plot shows the cutoff frequency versus the phase lead parameter m_2 . As m_2 increases, the frequency range for stability increases. A maximum is reached when $m_2=9$.

three coordinate axes (x , y , and z). Inductive sensors were used to measure the displacements of the piezoactuator and the signals were accessible through a custom signal access module (Figs. 1(a) and 5). The gain of the inductive sensors were $96 \mu\text{m}/\text{V}$ and $97 \mu\text{m}/\text{V}$ in the x -axis and y -axis, respectively. A PC computer and a data acquisition system running custom C code were used to implement the RC control system. The sampling frequency of the data acquisition and control hardware was 10 kHz.

The RC was applied to track a periodic reference trajectory in the x -axis as an illustrative example. This axis was the fast-scanning axis because the probe tip moves back and forth at least 100 times faster than the up and down motion in the y -direction during imaging. For example, a 100×100 pixel image requires the AFM tip to scan back and forth across the sample surface 100 times and slowly move from top to bottom (see Fig. 1(b)). It is noted that cross-coupling effects in piezotube actuators were not considered in this work. Interested readers are referred to the work of Tien et al. [39], for additional details to further improve tracking performance.

4.2 Modeling Piezoactuator Dynamics. A linear dynamics model of the piezoactuator was obtained for designing the RC system. The model was estimated from the measured frequency response function. The frequency response along the x -axis was measured using a dynamic signal analyzer (DSA, Hewlett Packard, Model 35670A). The response was measured over small

ranges to minimize the effects of hysteresis and above 1 Hz to avoid the effects of creep [6]. The resulting frequency response curves are shown in Fig. 6. A linear 12th-order transfer function model $G(s)$ (dash-dot line in Fig. 6) was curve fitted to the measured frequency response function. The continuous-time model was then converted to the discrete-time model $G_p(z)$ using the MATLAB function `c2d` with a sampling frequency of 10 kHz (shown by the dashed line in Fig. 6).

4.3 PID Control. Commercial SPMs use PID feedback controllers to minimize hysteresis, creep, and the effects of the vibrational dynamics [10]. Prior to integrating the RC, a PID controller was designed for the piezoactuator to control the motion along the x -axis. The PID controller is given by

$$G_c(z) = K_p + K_i \left(\frac{z}{z-1} \right) + K_d \left(\frac{z-1}{z} \right) \quad (14)$$

where the Ziegler–Nichols method [40] was used to tune the parameters of the controller to $K_p=1$, $K_i=1450$, and $K_d=0.0002$. The PID controller was implemented at a sampling frequency of 10 kHz. The performance of the PID controller to a step reference is shown in Fig. 7(a). It can be observed that without PID control, the open-loop response shows significant overshoot. Also, after 30 ms creep effect becomes noticeable. Creep is a slow behavior and after several minutes the tracking error can be in excess of 20%

Table 1 Stability of RC system for different low-pass filter cutoff frequencies and phase lead z^{m_2}

Phase lead m_2	Low-pass filter $Q(z)$'s cutoff frequency (Hz)				
	250	500	1000	2000	4000
0	Stable	Unstable	Unstable	Unstable	Unstable
2	Stable	Unstable	Unstable	Unstable	Unstable
4	Stable	Stable	Unstable	Unstable	Unstable
6	Stable	Stable	Stable	Unstable	Unstable
8	Stable	Stable	Stable	Stable	Stable

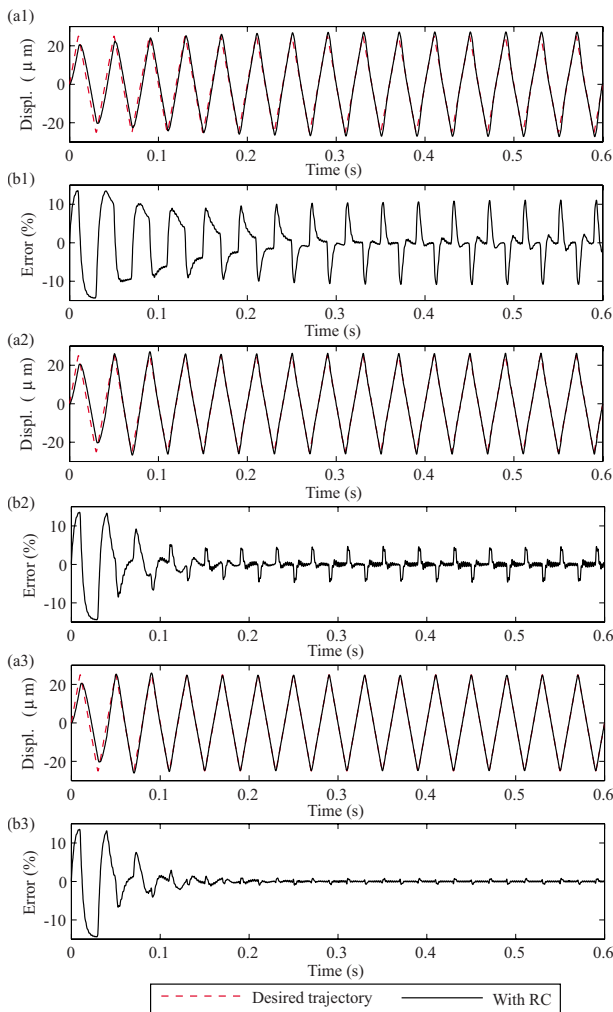


Fig. 9 Simulation results showing the tracking performance and error for scanning at 25 Hz, where (a1) and (b1) belong to RC with $k_{rc}=0.40$ and no phase lead; (a2) and (b2) belong to RC with phase lead $m_2=7$ and $k_{rc}=1.1$; (a3) and (b3) belong to RC with phase leads $m_1=6$, $m_2=7$, and $k_{rc}=1.1$.

[21]. On the other hand, the PID controller minimized the overshoot and creep effect.

The response of the PID controller for tracking a triangular trajectory at 1 Hz, 5 Hz, and 25 Hz are shown in Fig. 7(b). Triangle reference signals are commonly used in AFM imaging. The maximum tracking errors for the three cases are shown in Fig. 7(c). The error at 1 Hz (low speed) was relatively small, approximately 1.48% of the 10 μm range ($\pm 5 \mu\text{m}$). However, at 25 Hz (high speed) scanning the error was unacceptably large at 10.70%. Due to the vibrational dynamics and hysteresis effects, open-loop AFM imaging is limited to less than 2–3 Hz. The objective was to reduce the tracking error by adding a repetitive controller to the PID loop.

4.4 Simulation Study. Simulations were done to illustrate the design process and to study the effects of the RC's parameters on performance. The linear dynamics model $G_p(z)$ determined from the measured frequency response described above was used in the simulation. The first step is to design the low-pass filter and phase lead z^{m_2} for stability and robustness. Afterwards, the phase lead z^{m_1} was designed to minimize the steady-state tracking error. The steps are outlined as follows.

First, the RC was designed for stability and robustness. This involves designing a low-pass filter $Q(z)$ and adding phase lead

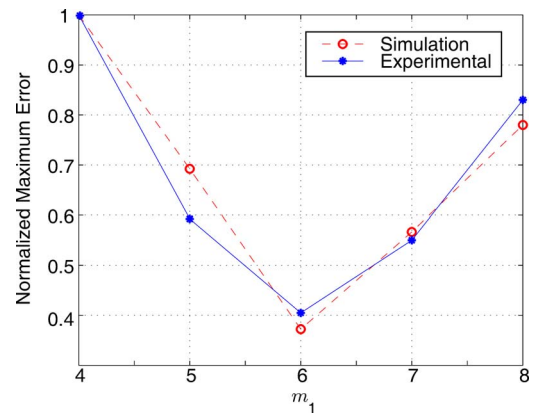


Fig. 10 Maximum error versus phase lead parameter m_1 . For the experiments, $m_1=6$ gave smallest error.

via m_2 to satisfy the conditions given by Eqs. (9) and (10). The following low-pass filter was used in the RC loop,

$$Q(z) = \frac{a}{z+b} \quad (15)$$

where $|a|+|b|=1$. The cutoff frequency ω_Q of the low-pass filter was chosen below the ± 90 deg crossover frequency to satisfy Eq. (10). The low-pass filter cutoff frequency is limited by the crossover frequency. Also, the cutoff frequency limits the achievable scan rate to about one-tenth of the cutoff frequency, i.e., $\omega_Q/10$.

The phase response $\theta_T(\omega)$ of the closed-loop feedback system without RC and different phase lead $\theta_2(\omega)$ are shown in Fig. 8. Without phase lead ($m_2=0$) the ± 90 deg crossover frequency was approximately 486 Hz. This value sets the maximum cutoff frequency for the low-pass filter and the maximum scan rate.

Next, simulations were done to show the tracking performance of RC. The chosen cutoff frequency for $Q(z)$ was 250 Hz and zero-phase lead ($m_2=0$) was used. Therefore, the maximum scan rate is 25 Hz. It is noted that for higher rate scanning, the cutoff can be increased, but only up to 486 Hz when $m_2=0$ (see Fig. 8). The 250 Hz cutoff frequency was chosen because it provided a safety margin of approximately 2. Then, the RC gain was determined by satisfying Eq. (9), for instance picking $k_{rc}=0.40$. The simulated tracking response for $\pm 25 \mu\text{m}$ scan range at 25 Hz is shown in Fig. 9. The first two plots, Figs. 9(a1) and 9(b1), show the tracking performance and error, respectively, for a stable RC system without any phase lead compensators, i.e., $m_1=m_2=0$. In this case, increasing k_{rc} and/or the low-pass filter's cutoff frequency caused instability. Reducing the RC gain, however, reduced the convergence rate. The steady-state tracking error was minimally affected by the RC gain and the phase lead through m_2 .

The scan rate can be improved by increasing the ± 90 deg crossover frequency by adding phase lead through the parameter m_2 . The inset in Fig. 8 shows the ± 90 deg crossover frequency versus the phase lead parameter m_2 .

With the addition of phase lead, such as $m_2=7$, the ± 90 deg crossover frequency was increased to approximately 2000 Hz. Therefore, the low-pass filter's cutoff frequency can be improved to raise the RC's bandwidth permitting tracking of higher frequency components. Subsequently, the RC gain Eq. (9) can be increased. For example with $m_2=7$, $k_{rc}=1.1$, and simulation results are shown in Figs. 9(a2) and 9(b2) that demonstrate improvement in the convergence rate and reduced tracking error compared with the previous case without phase lead z^{m_2} . As indicated in the inset plot in Fig. 8, the higher values of m_2 show no improvement in the crossover frequency.

Simulations were done with $k_{rc}=0.4$ to verify the stability of the closed-loop system with RC for different low-pass filter cutoff

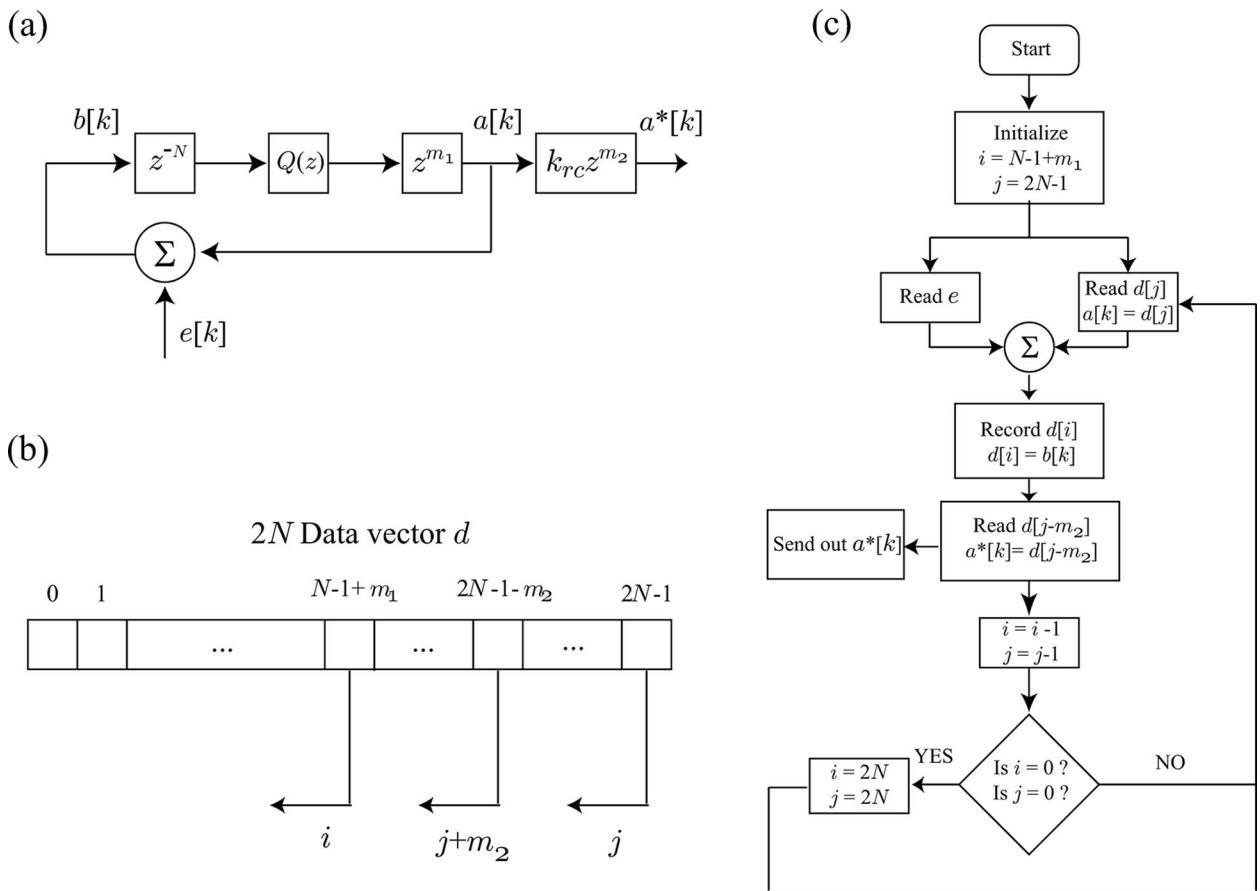


Fig. 11 Digital implementation of repetitive control: (a) Equivalent discrete-time block diagram of the RC loop, (b) linear data vector for implementing the one-period delay and the phase lead compensators, and (c) the flow diagram for implementing the RC loop

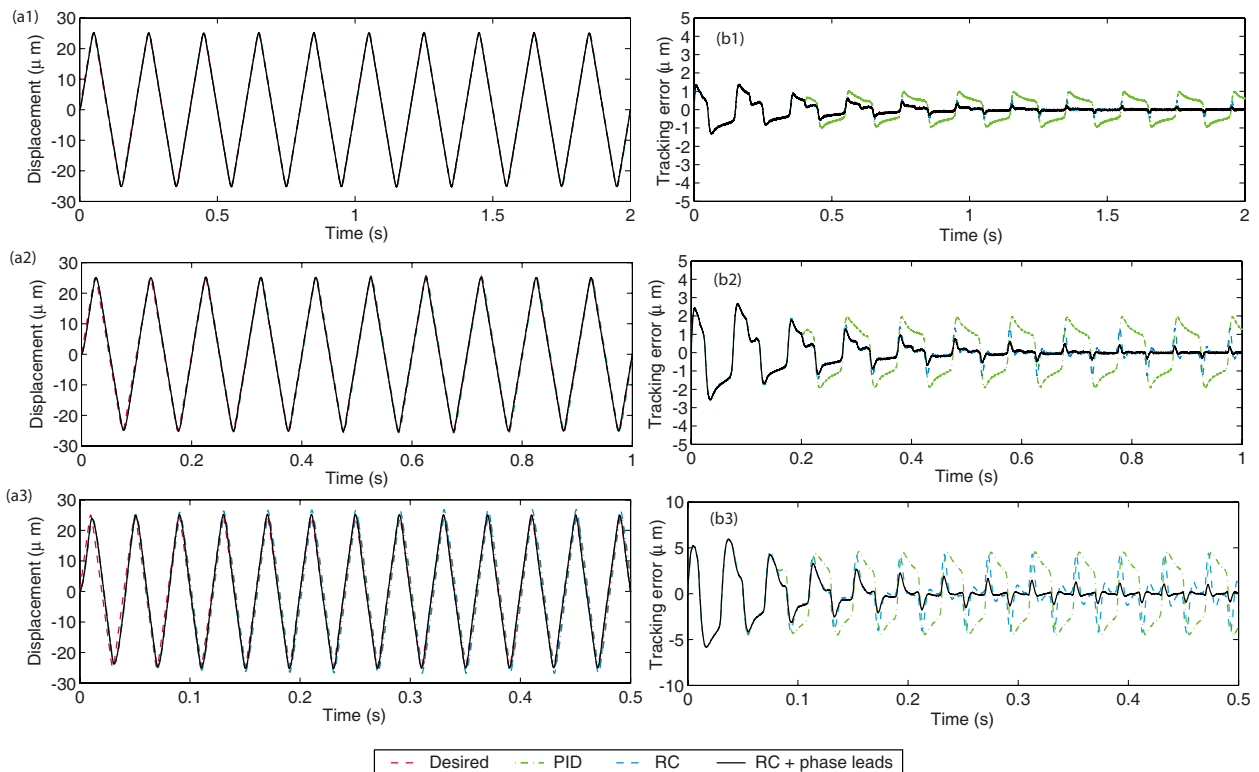


Fig. 12 Experimental tracking response and error for PID (dash-dot), RC (dashed line), and RC with phase lead compensation ($m_1=6$ and $m_2=0$) (solid line) for 5 Hz (a1 and b1), 10 Hz (a2 and b2), and 25 Hz (a3 and b3) scanning

Table 2 Tracking results for $\pm 25 \mu\text{m}$ range

Controller	5 Hz		10 Hz		25 Hz	
	e_{\max} (%)	e_{rms} (%)	e_{\max} (%)	e_{rms} (%)	e_{\max} (%)	e_{rms} (%)
PID	2.01	1.28	3.99	2.61	9.16	6.61
RC	0.96	0.21	2.74	0.79	8.86	3.69
RC+phase leads	0.43	0.08	0.46	0.10	1.78	0.57

frequencies and values of m_2 . The results are summarized in Table 1. Comparing the inset plot in Fig. 8 and the summary in Table 1, with $m_2=0$ the closed-loop RC system is stable when the low-pass filter frequency is below the crossover frequency of 486 Hz. As the cutoff frequency increases, for example at 500 Hz and above, the RC system is unstable. But the stability can be achieved by adding phase lead through m_2 as shown by the results in Table 1.

Finally, by adding phase lead using z^{m_1} in the RC loop, for example $m_1=6$, the maximum tracking error, defined as

$$e_{\max}(\%) = \left[\frac{\max|y - r|}{\max(y) - \min(y)} \right] \times 100\% \quad (16)$$

where y and r are the measured and reference outputs, respectively, was substantially reduced from 11.96% and 5.32% (Figs. 9(a2) and 9(b2)) to 0.97% of the total range (50 μm) as illustrated in Figs. 9(a3) and 9(b3). The phase lead in the RC loop increases the magnitude of the gain of the RC at the scanning signal's harmonics, hence reducing the size of $W(e^{jk\omega_p})$ (Eq. (13)).

The optimum value of the phase lead m_1 was determined by looking at the maximum error versus m_1 . The simulation results are shown in Fig. 10, plotted as normalized maximum error versus m_1 , along with experimental results which will be discussed in the following section. As shown in the figure, the optimum value is $m_1=6$ and this value was also used in the experiments discussed below.

4.5 Experimental Implementation. Two repetitive controllers were designed, implemented, and their responses are compared to PID control. The first is a standard RC with a low-pass filter $Q(z)$ in the RC loop. The standard RC did not include phase lead compensators. The second RC contains the two phase lead compensators z^{m_1} and z^{m_2} to improve the tracking performance and stability, respectively.

In the experiment, the reference signal was a $\pm 25 \mu\text{m}$ triangle wave at 5 Hz, 10 Hz, and 25 Hz. The reference trajectory was

passed through a two-pole zero-phase-shift filter with a cutoff frequency of 250 Hz to remove high-frequency components before applying it to the closed-loop system. Triangle scan signals are typically used for AFM imaging and they were filtered to avoid exciting high-frequency dynamics. The cutoff frequency for the low-pass filter $Q(z)$ in the RC loop was set at 250 Hz. Due to hardware limitations where the sampling frequency was 10 kHz, $m_2=0$ was chosen to give a maximum scan frequency of 25 Hz. The RC gain was chosen as $k_{rc}=0.40$ and this value satisfied the condition given by Eq. (9).

Let N be an integer value representing the delay period, the ratio of signal period T_p to the sampling period T_s . Figure 11(a) shows the equivalent discrete-time block diagram for the RC loop, where z^{-N} is a delay of period N . The two phase lead compensators, z^{m_1} and z^{m_2} , have leads of $m_1=6$ and $m_2=0$. Both the delay and phase leads were implemented using a linear data vector d as shown in Fig. 11(b) with $2N$ elements. Two counters i and j were used, one controlled the location where incoming data was stored to the data vector and the other controlled the location where data was read and sent. The difference in the indices i and j determines the overall delay $-N+m_1+m_2$, and since $N \gg m_1+m_2$, the delay implementation was causal. The flow diagram for the RC implementation with respect to the linear data vector d is shown in Fig. 11(c). Upon reaching the end of the array at $i=0$ and $j=0$, both indices were reset to $2N-1$ and the process was repeated.

5 Experimental Results and Discussion

The tracking results for the PID, regular RC, and the RC with the phase lead compensators for $\pm 25 \mu\text{m}$ scanning at 5 Hz, 10 Hz, and 25 Hz are presented in Fig. 12 and Table 2. The steady-state tracking errors, measured at the last two cycles, are reported as a percentage of the range of motion. In particular, the maximum error Eq. (16) and the root-mean-squared error defined as

$$e_{\text{rms}}(\%) = \left[\frac{\sqrt{\frac{1}{T} \int_0^T [y(t) - r(t)]^2 dt}}{\max(y) - \min(y)} \right] \times 100\% \quad (17)$$

are reported.

Because the action of the repetitive controller is delayed by one scan period, the tracking response for the first period are similar for the PID, RC, and RC with phase lead compensation as shown in Fig. 12. However, after the first period the RC begins to take action as illustrated by the reduction in the tracking error from one cycle to the next. On the other hand, the tracking error of the PID controller persists from one cycle to the next.

The 5 Hz scanning results shown in Figs. 12(a1) and 12(b1), and Table 2 demonstrate that the regular RC controller reduced the maximum tracking error from 2.01% to 0.96% compared to the PID controller, a 52% reduction. By using RC with the phase lead compensation, an additional 55% improvement in tracking performance was achieved. In this case, the maximum tracking error is 0.43%.

At 25 Hz, the tracking error of PID was unacceptably large at 9.16%. In fact, for AFM scanning operations the maximum track-

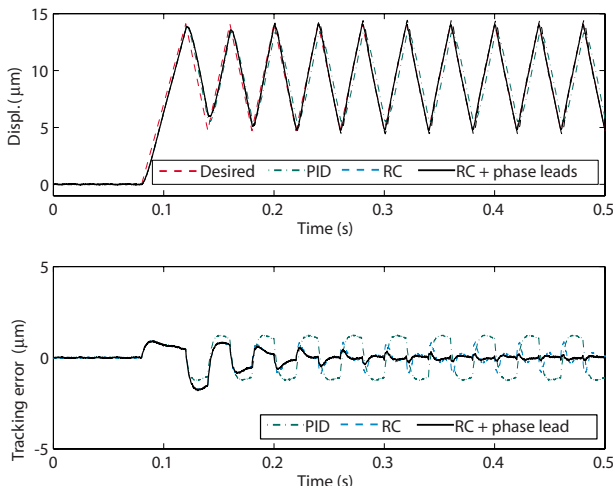


Fig. 13 Tracking results for offset triangle scan at 25 Hz

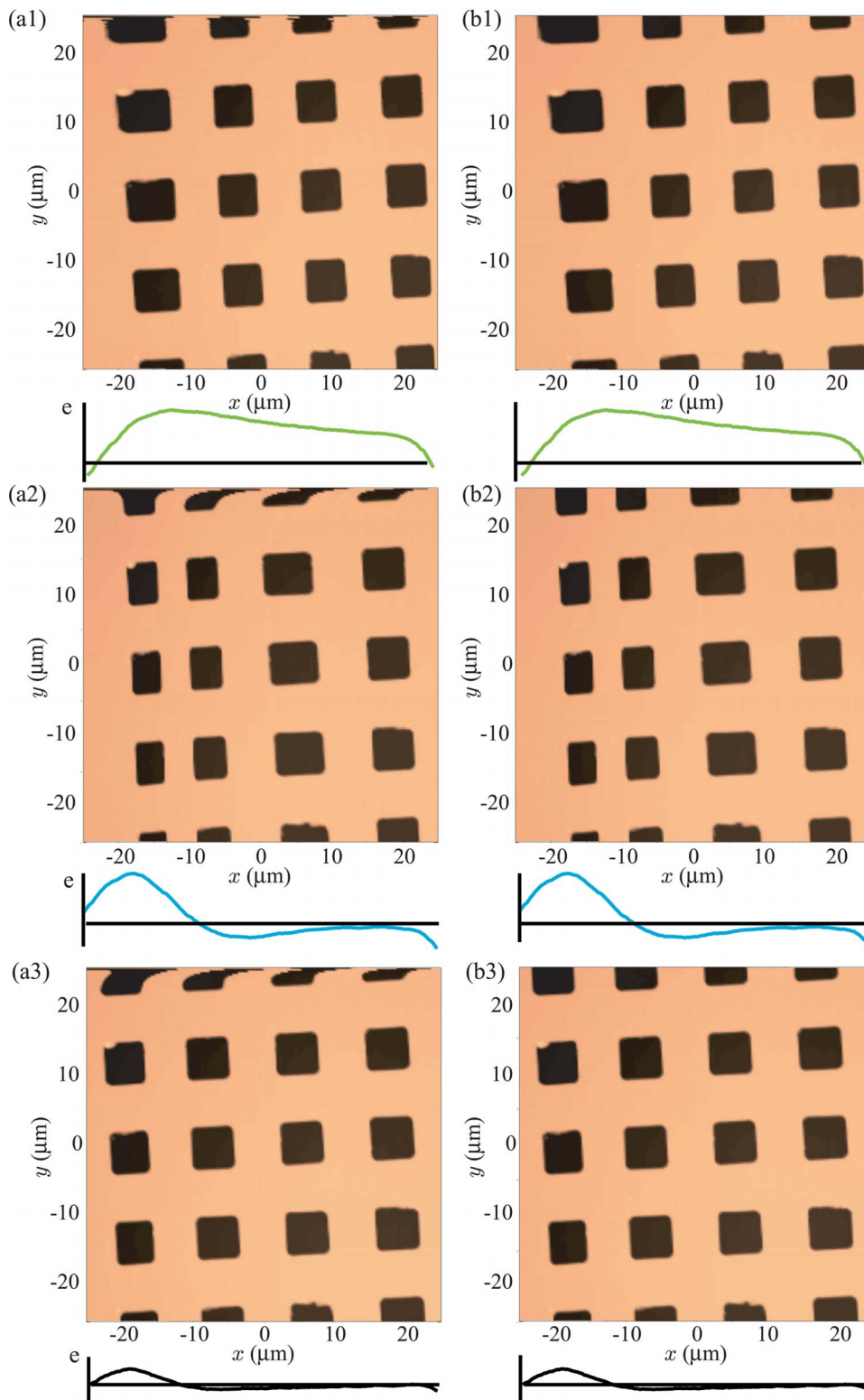


Fig. 14 Atomic force microscope images using measured tracking response along the x -axis at 25 Hz and $\pm 25 \mu\text{m}$ range. Steady-state tracking error shown below each image. PID control (a1) first pass and (b1) second pass; standard RC (a2) first pass and (b2) second pass; and RC with phase lead compensators ($m_1=6$ and $m_2=0$) (a3) first pass and (b3) second pass. The x -axis is the fast-scanning motion and tip starts at the top and slowly scans down along the y -axis.

ing error should be less than a few percent. The results in Table 2 show that the regular plug-in RC controller was not able to improve the tracking performance at 25 Hz. However, the RC with

phase lead compensation gives lower maximum tracking error at 1.78%. Therefore, the RC with phase lead compensation enables precision tracking at higher scan rates. The optimum value of the

phase lead via m_1 was chosen using the simulation results in Fig. 10. The simulation results were validated in the experiments as shown in the figure, where $m_1=6$ gives the lowest steady-state tracking error.

Next, scanning offset from the piezoactuator's center position is demonstrated as shown in Fig. 13. For this offset scanning operation, the PID controller accounted for the low frequency dynamics such as creep and the RC was used for tracking the periodic trajectory. The tracking results in Fig. 13 show that the RC was effective at minimizing the tracking error.

5.1 Effects on AFM Imaging. To study the effects of RC on AFM imaging, the measured tracking response of the PID and the two repetitive controllers were used to obtain simulated images of a calibration sample. The number of cycles was set to 200 to produce 200×200 pixels image. The data for the vertical profile of the calibration sample were first obtained with the AFM under PID feedback control at a 1 Hz scan rate (512×512 pixels). The imaging mode used was constant-height, contact mode with a relatively low force set-point. Using the measured x -axis tracking response from the controllers, simulated AFM images were obtained and for this study, they were preferred over obtaining the images experimentally to minimize artifacts in the images caused by coupling effects. A reference 512×512 pixels image measured at 1 Hz was used to simulate the image from the PID, RC, and RC with phase lead. The image simulation was done using MATLAB's 2D interpolation function `interp2`. The measured tracking response along the x -axis for PID and the two RC's were used by the interpolation function to obtain the vertical profile of the calibration sample.

The resulting images using the measured reference image and the measured tracking performance are shown in Fig. 12 for scanning at 25 Hz. In particular, the left-hand column shows images for the first pass and on the right-hand column are images from the second pass. For the images on the left-hand column, the top of each image shows distortion caused by transients where the starting point was $x=0$. After a few cycles, the images from the PID controller begin to reach steady state (Fig. 12(a1)), but the features continue to appear distorted. Specifically, the size and shape of the dark areas are more elongated at the turn-around on the left-hand side of the image compared to the right-side of the image. As expected, the PID image on the second pass remains unchanged because the tracking error with PID repeats from one cycle to the next.

With standard RC (without phase lead compensation), the images are noticeably distorted as shown in Figs. 14(a2) and 14(b2). Although the root-mean-squared error for standard RC is nearly half of the PID controller (see Table 2), the large maximum error shows that distortion in the AFM image is still significant. On the other hand, the improved RC with phase lead compensation produces images with no noticeable distortion. On the first pass, the top of the image in Fig. 14(a3) shows initial distortion, but after a few cycles the image quality improves and remains the same for the second pass as illustrated in Fig. 14(b3). These results indicate that RC with phase lead compensation can be used to achieve precise tracking in AFM for low-distortion imaging.

6 Conclusions

The design and implementation of a repetitive controller with phase lead compensation for AFM were presented. The RC was combined with a PID feedback system for precision tracking of periodic trajectories. It was shown that one phase lead compensator affected the stability and robustness of the RC closed-loop system; and the other affected the steady-state tracking precision. Experimental results showed that at 25 Hz scan rate, the maximum error was less than 2% using the improved RC technique, where as PID control resulted in 9.16% tracking error. The AFM images based on the measured tracking results at 25 Hz scan rate showed that RC can be used to obtain low-distortion AFM im-

ages. Unlike PID control, which produces distorted images from one frame to the next, the RC produced AFM images with negligible distortion after the first frame.

Acknowledgment

This work was supported, in part, by the National Science Foundation Grants (DUE Contract No. 0633098 and CMMI Contract No. 0726778).

References

- [1] Salapaka, S. M., and Salapaka, M. V., 2008, "Scanning Probe Microscopy," *IEEE Control Syst. Mag.*, **28**(2), pp. 65–83.
- [2] Jalili, N., and Laxminarayana, K., 2004, "A Review of Atomic Force Microscopy Imaging Systems: Application to Molecular Metrology and Biological Sciences," *Mechatronics*, **14**(8), pp. 907–945.
- [3] Campbell, P. M., and Snow, E. S., 1996, "Proximal Probe-Based Fabrication of Nanostructures," *Semicond. Sci. Technol.*, **11**, (1s), pp. 1558–1562.
- [4] Barrett, R. C., and Quate, C. F., 1991, "Optical Scan-Correction System Applied to Atomic Force Microscopy," *Rev. Sci. Instrum.*, **62**(6), pp. 1393–1399.
- [5] Hu, H., and Mrad, R. B., 2002, "On the Classical Preisach Model for Hysteresis in Piezoceramic Actuators," *Mechatronics*, **13**(2), pp. 85–94.
- [6] Croft, D., Shed, G., and Devasia, S., 2001, "Creep, Hysteresis, and Vibration Compensation for Piezoactuators: Atomic Force Microscopy Application," *ASME J. Dyn. Syst., Meas., Control*, **123**, pp. 35–43.
- [7] Francis, B. A., and Wonham, W. M., 1976, "The Internal Model Principle of Control Theory," *Automatica*, **12**(5), pp. 457–465.
- [8] Inoue, T., Nakano, M., and Iwai, S., 1981, "High Accuracy Control of a Proton Synchrotron Magnet Power Supply," *Proceedings of the Eighth World Congress IFAC*, pp. 216–221.
- [9] Hara, S., Yamamoto, Y., Omata, T., and Nakano, M., 1988, "Repetitive Control System: A New Type Servo System for Periodic Exogenous Signals," *IEEE Trans. Autom. Control*, **33**(7), pp. 659–668.
- [10] Abramovitch, D. Y., Andersson, S. B., Pao, L. Y., and Schitter, G., 2007, "A Tutorial on the Mechanisms, Dynamics, and Control of Atomic Force Microscopes," *American Control Conference*, New York, pp. 3488–3502.
- [11] Chew, K. K., and Tomizuka, M., 1990, "Digital Control of Repetitive Errors in Disk Drive Systems," *IEEE Control Syst. Mag.*, **10**(1), pp. 16–20.
- [12] Steinbuch, M., Weiland, S., and Singh, T., 2007, "Design of Noise and Period-Time Robust High-Order Repetitive Control, With Application to Optical Storage," *Automatica*, **43**(12), pp. 2086–2095.
- [13] Michels, L., Pinheiro, H., and Grundling, H. A., 2004, "Design of Plug-In Repetitive Controllers for Single-Phase PWM Inverters," *IEEE Industry Applications Annual Conference*, 1, pp. 163–170.
- [14] Li, C. J., and Li, S. Y., 1996, "To Improve Workpiece Roundness in Precision Diamond Turning by In Situ Measurement and Repetitive Control," *Mechatronics*, **6**(5), pp. 523–535.
- [15] Chen, S.-L., and Hsieh, T.-H., 2007, "Repetitive Control Design and Implementation for Linear Motor Machine Tool," *Int. J. Mach. Tools Manuf.*, **47**(12–13), pp. 1807–1816.
- [16] Ghosh, J., and Paden, B., 2000, "Nonlinear Repetitive Control," *IEEE Trans. Autom. Control*, **45**(5), pp. 949–953.
- [17] Choi, G. S., Lim, Y. A., and Choi, G. H., 2002, "Tracking Position Control of Piezoelectric Actuators for Periodic Reference Inputs," *Mechatronics*, **12**(5), pp. 669–684.
- [18] Rifai, O. M. E., and Youcef-Toumi, K., 2002, "Creep in Piezoelectric Scanners of Atomic Force Microscopes," *Proceedings of American Control Conference, Anchorage, AK*, pp. 3777–3782.
- [19] Arimoto, S., Kawamura, S., and Miyazaki, F., 1984, "Bettering Operation of Robots by Learning," *J. Rob. Syst.*, **1**(2), pp. 123–140.
- [20] Moore, K. L., Dahleh, M., and Bhattacharyya, S. P., 1992, "Iterative Learning Control: A Survey and New Results," *J. Rob. Syst.*, **9**(5), pp. 563–594.
- [21] Leang, K. K., and Devasia, S., 2006, "Design of Hysteresis-Compensating Iterative Learning Control for Piezo Positioners: Application to Atomic Force Microscopes," *Mechatronics*, **16**(3–4), pp. 141–158.
- [22] Wu, Y., and Zou, Q., 2007, "Iterative Control Approach to Compensate for Both the Hysteresis and the Dynamics Effects of Piezo Actuators," *IEEE Trans. Control Syst. Technol.*, **15**(5), pp. 936–944.
- [23] Hill, M. D., White, G. S., Hwang, C.-S., and Lloyd, I. K., 1996, "Cyclic Damage in Lead Zirconate Titanate," *J. Am. Ceram. Soc.*, **79**(7), pp. 1915–1920.
- [24] Lowrie, F., Cain, M., Stewart, M., and Gee, M., 1999, "Time Dependent Behaviour of Piezo-Electric Materials," *National Physical Laboratory Technical Report No. 151*.
- [25] Lee, H.-J., and Saravanas, D. A., 1998, "The Effect of Temperature Dependent Material Properties on the Response of Piezoelectric Composite Materials," *J. Intell. Mater. Syst. Struct.*, **9**(7), pp. 503–508.
- [26] Fantner, G. E., Hegarty, P., Kindt, J. H., Schitter, G., Cidade, A. G. A., and Hansma, P. K., 2005, "Data Acquisition System for High-Speed Atomic Force Microscopy," *Rev. Sci. Instrum.*, **76**(2), p. 026118.
- [27] Schitter, G., Astrom, K. J., DeMartini, B. E., Thurner, P. J., Turner, K. L., and Hansma, P. K., 2007, "Design and Modeling of a High-Speed AFM-Scanner," *IEEE Trans. Control Syst. Technol.*, **15**(5), pp. 906–915.
- [28] Leang, K. K., and Fleming, A. J., 2009, "High-Speed Serial-Kinematic AFM

- Scanner: Design and Drive Considerations,” *Asian J. Control*, **11**(2), pp. 144–153.
- [29] Leyva-Ramos, J., Escobar, G., Martinez, P. R., and Mattavelli, P., 2005, “Analog Circuits to Implement Repetitive Controllers for Tracking and Disturbance Rejection of Periodic Signals,” *IEEE Trans. Circuits Syst.*, **52**(8), pp. 466–470.
- [30] Tomizuka, M., Tsao, T. C., and Chew, K. K., 1988, “Discrete Time Domain Analysis and Synthesis of Repetitive Controllers,” *American Control Conference*, pp. 860–866.
- [31] Ratcliffe, J. D., Lewin, P. L., and Rogers, E., 2005, “Stable Repetitive Control by Frequency Aliasing,” *Intelligent Control Systems and Optimization*, pp. 323–326.
- [32] Broberg, H. L., and Molyet, R. G., 1994, “A New Approach to Phase Cancellation in Repetitive Control,” *IEEE Industry Applications Society Annual Meeting*, Vol. 3, pp. 1766–1770.
- [33] Wang, Y., Wang, D., Zhang, B., Zhou, K., and Ye, Y., 2006, “Robust Repetitive Control With Linear Phase Lead,” *American Control Conference*, Minneapolis, MN, Vol. 2006, pp. 232–237.
- [34] Yamada, M., Riadh, Z., and Funahashi, Y., 1999, “Design of Discrete-Time Repetitive Control System for Pole Placement and Application,” *IEEE/ASME Trans. Mechatron.*, **4**(2), pp. 110–118.
- [35] Zhou, K., and Doyle, J. C., 1998, *Essentials of Robust Control*, Prentice-Hall, Englewood Cliffs, NJ.
- [36] Leang, K. K., and Devasia, S., 2007, “Feedback-Linearized Inverse Feedforward for Creep, Hysteresis, and Vibration Compensation in AFM Piezoactuators,” *IEEE Trans. Control Syst. Technol.*, **15**(5), pp. 927–935.
- [37] Ahn, H.-S., 2003, “Design of a Repetitive Control System for a Piezoelectric Actuator Based on the Inverse Hysteresis Model,” *The Fourth International Conference on Control and Automation*, Montreal, Canada, pp. 128–132.
- [38] Shan, Y., and Leang, K. K., 2009, “Repetitive Control With Prandtl-Ishlinskii Hysteresis Inverse for Piezo-Based Nanopositioning,” *American Control Conference*, St. Louis, MO.
- [39] Tien, S., Zou, Q., and Devasia, S., 2005, “Iterative Control of Dynamics-Coupling-Caused Errors in Piezoscanners During High-Speed AFM Operation,” *IEEE Trans. Control Syst. Technol.*, **13**(6), pp. 921–931.
- [40] Franklin, G. F., Powell, J. D., and Emami-Naeini, A., 2006, *Feedback Control of Dynamic Systems*, 5th ed.